International Journal of Steel Structures
https://doi.org/10.1007/s13296-023-00781-9

Online ISSN 2093-6311
Print ISSN 1598-2351

Practical ANN Model for Estimating Buckling Load Capacity of Corroded Web-Tapered Steel I-Section Columns

Trong-Ha Nguyen[1] · Van-Tien Phan[1] · Duy-Duan Nguyen[1]

Received: 25 November 2022 / Accepted: 18 September 2023

Abstract

This study develops an artificial neural network (ANN) to estimate the critical buckling load (CBL) of corroded web-tapered steel I-section (WTSI) columns in pre-engineered steel buildings. A total of 387 datasets are employed to develop the ANN model. The datasets are generated from the proposed analytical model and Newton–Raphson method. The input parameters of the developed ANN model contain the cross-sectional dimensions of the steel column (i.e., the top and bottom flange width, top and bottom flange thickness, maximum section height, minimum section height, and web thickness), elastic modulus of material, and the column height. Meanwhile, the CBL is the output parameter of the ANN model. A predictive process for the CBL of the corroded WTSI columns has been proposed based on the ANN model and previous corrosion model. Results reveal that the ANN model showed an excellent performance in predicting the CBL of the corroded steel columns. The R^2 values of the training, testing, and validation data are 0.99975, 0.99916, and 0.99951, respectively. The root-mean-squared errors of the training, testing, and validation data are 96.705 (kN), 103.402 (kN), and 103.200 (kN), respectively. Additionally, the a20-index is very close to 1.0. Moreover, a graphical user interface tool is constructed to facilitate the CBL calculation of the corroded WTSI columns.

Keywords Corroded web-tapered steel I-section column · Artificial neural network · Critical buckling load · Predicted formula · Graphical user interface

1 Introduction

The web-tapered steel I-section (WTSI) beams and columns have been commonly utilized in steel structures since it possesses an optimization of structural cross-section, as shown in Fig. 1. Nevertheless, current code provisions do not provide specific guidelines for designing non-uniform members as WTSI columns (Li, 2008), even in Eurocode 3 (CEN 2005). Therefore, structural designers have been struggling with the determination of the critical buckling load (CBL) of the web-tapered section members (Marques et al., 2012, 2014a, b; Simões da Silva et al., 2010). Moreover, previous works pointed out that it is required to investigate the linear, nonlinear analyses, and buckling failure of off-center steel structures subjected to various loading scenarios (Andalib et al., 2014, 2018a, b; Bazzaz et al., 2012, 2014, 2015a, b).

The assessment of corrosion effects on the performance of the mentioned structure is recommended in EN ISO: 9223 and other design standards (Eurocode, 1996; Gardner & Nethercot, 2005; Standard, 2002). These recommendations depend on each standard. Determination of the load-bearing capacity of steel structures considering effects of corrosion is an interest topic to researchers. Reliability assessments and global sensitivity analyses of the steel–concrete composite beams considering metal corrosion was conducted by Tran et al. (2020). Landolfo et al. (2010) carried out a systematic review on the modeling of corrosion damage of the metal structures. Seccer et al. (2017) assessed the damage of steel frames due to bending considering metal corrosion. Besides, several studies proposed methods to evaluate the reliability of steel frames under different metal corrosion scenarios (Ha, 2019; Ngoc-Long & Ha, 2020; Tran & Nguyen, 2021). However, a specific procedure has not

✉ Duy-Duan Nguyen
duyduankxd@vinhuni.edu.vn

Trong-Ha Nguyen
trongha@vinhuni.edu.vn

Van-Tien Phan
vantienkxd@vinhuni.edu.vn

[1] Department of Civil Engineering, Vinh University, Vinh 461010, Vietnam

Published online: 07 October 2023

Fig. 1 Examples of the WTSI columns in real pre-engineering steel buildings

been provided for determining the CBL of corroded steel columns.

Nowadays, machine learning (ML) algorithms have been employed in solving many problems of civil engineering field (Flah et al., 2021; Ilter et al., 2020; Naser, 2023; Reich, 1997; Thai, 2022; Vadyala et al., 2022). For steel structures, there are numerous studies that have been performed so far. In the study of Nguyen et al. (2021a), the authors utilized artificial neural network (ANN) and adaptive neural fuzzy-based system model to propose a formula to determine the bearing capacity of cold-formed steel columns with oval hollow sections. Nguyen et al. (2021b) also applied the ANN model to predict the CBL of web tapered I-section steel columns, however, this study considered both pinned ends of steel columns. ANN algorithm was also applied for estimating the maximum speed of vehicle moving on the steel girders bridge accounting for corrosion (Tran et al., 2022). They pointed out that the vehicle speed limit was significantly reduced if considering the corrosion of the steel girder. In addition, applying ANN to predict the bearing capacity of other structures were studied elsewhere (Nguyen et al., 2021a, b, c; Tran & Kim, 2020; Tran et al., 2019; Vakhshouri & Nejadi, 2018).

Moreover, the prediction of atmosphere corrosion rate of steel has been performed using both theoretically and experimentally. Tidblad (2012) predicted atmospheric corrosion rate accounting for various environmental conditions such as temperature, time of wetness, pollutant concentration, exposing time, and relative humidity. The linear quantitative relationships of environmental parameters and corrosion rates was proposed in (Knotkova et al., 1995; Morcillo, 1995). Other quantitative relationships such as dose–response functions (Kucera et al., 2007; Mikhailov et al., 2004; Tidblad et al., 2001) and basic log-linear models (Knotkova et al., 1995, 2002; Komp, 1987; Panchenko & Marshakov, 2017; Roberge et al., 2002) were established. In addition, some models based on experimental results were also proposed (Chico et al., 2017; Knotkova et al., 2002; Roberge et al., 2002). In different metal atmospheric corrosion models proposed above, the corrosion model developed by Komp (1987) has proven to be reliable and easy to use. Therefore, this model was widely used in many studies (Landolfo et al., 2010; Tran & Nguyen, 2021; Secer & Uzun, 2017).

The aim of this study is to develop an ANN model for calculating the CBL of corroded WTSI columns in pre-engineered steel buildings. Corrosion model is adopted based on the model developed by Komp (1987). The ANN model is constructed based on a set of 387 data sets, which are generated using the analytical and Newton–Raphson methods. Input variables for the ANN model are the column height (H), the maximum cross-section height of column ($h_{c,\max}$), the minimum cross-section height of column ($h_{c,\min}$), the flange width (b_f), the flange thickness (t_f), the web thickness (t_w), the bay width of frame (L_b), the maximum cross-section height of beam ($h_{b,\max}$), the minimum cross-section height of beam ($h_{b,\min}$), and elastic modulus of material (E). Meanwhile the output of ANN is the CBL of the corroded steel column. Moreover, a graphical user interface (GUI) based on MATLAB is developed for facilitating the practical design process of the corroded WTSI columns.

2 Analytical Model of CBL of WTSI Columns

Considering a pre-engineered industrial steel frame, which is shown in Fig. 1. The calculated model of the steel frame is assumed as a column with a pinned end and a clamped guided end, as also shown in Fig. 2. The differential equation of buckling of columns is expressed by Eq. (1) (Nguyen, 2007).

$$EI_{c,\min}\left(\frac{z}{a}\right)^2\frac{d^2y}{dz^2}+Py=0 \quad (1)$$

By solving Eq. (1) and considering boundary conditions, it can be obtained the following expression:

$$\left[1-2(a+H)P\overline{\varphi}\right]\tan\left(\gamma\ln\frac{a+H}{a}\right)+2\gamma=0 \quad (2)$$

where $\overline{\varphi}$ is the elastic coefficient of the beam-column connection, determined by Eq. (3); γ is calculated by Eq. (4).

$$\overline{\varphi}=\frac{H}{EI_{b,\min}}\frac{1}{\left(\frac{h_{b,\max}}{h_{b,\min}}-1\right)^3}\left[\frac{h_{b,\max}}{h_{b,\min}}-2\ln\left(\frac{h_{b,\max}}{h_{b,\min}}\right)-\frac{1}{\frac{h_{b,\max}}{h_{b,\min}}}\right] \quad (3)$$

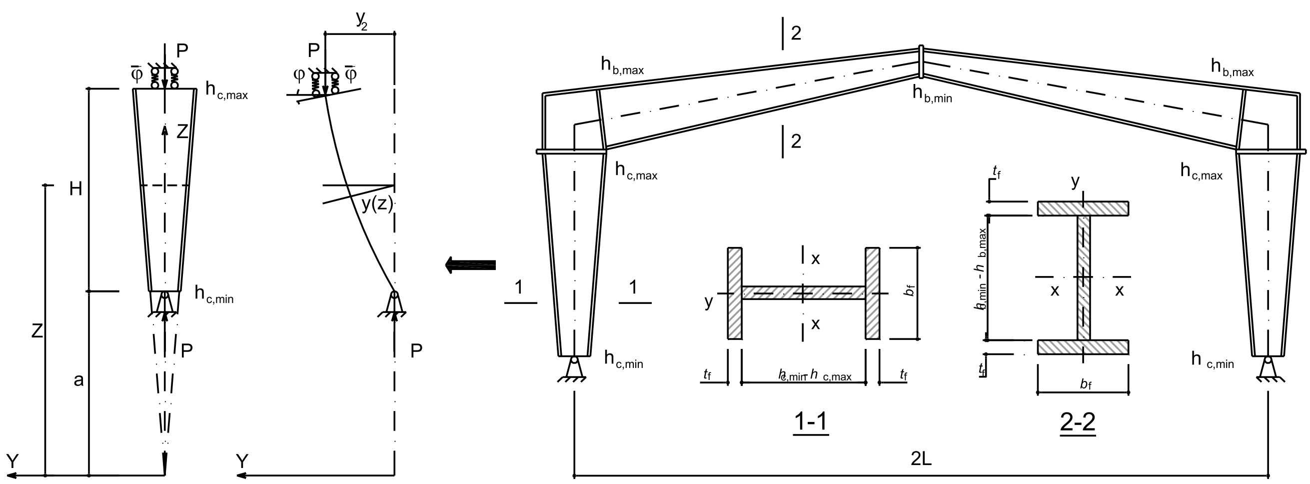

Fig. 2 Web-tapered steel I-section frame with flexible beam-column joint

$$\gamma^2 = \frac{Pa^2}{EI_{c,\min}} - \frac{1}{4} \tag{4}$$

Equation (4) can be rewritten as

$$P = \left(\gamma^2 + \frac{1}{4}\right)\frac{EI_{c,\min}}{a^2} \tag{5}$$

By setting $\overline{\varphi} = \overline{\varphi'}\frac{H}{EI_{c,\min}}$ and substituting Eq. (5) into Eq. (2), we obtained:

$$\left[1 - 2\left(\frac{a+H}{a}\right)\frac{H}{a}\left(\gamma^2 + \frac{1}{4}\right)\overline{\varphi'}\right]\tan\left(\gamma \ln \frac{a+H}{a}\right) + 2\gamma = 0 \tag{6}$$

For a symmetry of I-sections (i.e., the same top and bottom flanges), Eq. (6) can be rewritten as

$$\left[1 - 2\frac{h_{c,\max}}{h_{c,\min}}\left(\frac{h_{c,\max}}{h_{c,\min}} - 1\right)\left(\gamma^2 + \frac{1}{4}\right)\overline{\varphi'}\right]\tan\left(\gamma \ln \frac{h_{c,\max}}{h_{c,\min}}\right) + 2\gamma = 0 \tag{7}$$

Where

$$\overline{\varphi'} = \left[\frac{2\gamma}{\tan\left(\gamma \ln \frac{h_{c,\max}}{h_{c,\min}}\right)} + 1\right]\frac{1}{2\frac{h_{c,\max}}{h_{c,\min}}\left(\frac{h_{c,\max}}{h_{c,\min}} - 1\right)\left(\gamma^2 + \frac{1}{4}\right)} \tag{8}$$

For a specific value of $\frac{h_{c,\max}}{h_{c,min}}$ and $\bar{\varphi}'$, based on Eq. (7), γ is calculated. Finally, the critical buckling load is then determined by Eq. (5). However, it is challenged to solve the transcendental Eq. (7) analytically, thus it should be solved using numerical methods such as Newton–Raphson. Each solution of γ corresponds to a buckling mode of the steel column. The minimal value of γ is corresponding to the CBL of the columns.

3 Data Generation

To generate the data sets for ANN model, a wide range of input parameters is conducted, in which the inputs are the column height (H), the maximum cross-section height of column ($h_{c,\max}$), the minimum cross-section height of column ($h_{c,\min}$), the flange width (b_f), the flange thickness (t_f), the web thickness (t_w), the maximum cross-section height of beam ($h_{b,\max}$), the minimum cross-section height of beam ($h_{b,\min}$), the bay width of frame (L_b), elastic modulus of material (E). As a result, a set of 387 data samples was analytically created to develop ANN models. The statistical properties and histograms of generated data sets are shown in Table 1 and Fig. 3, respectively.

Figure 4 describes the calculated correlation coefficients between parameters. It is observed that the relationship between input and output parameters is small. The largest correlation relationship between $h_{c,\max}$ and P_{cr} is only 0.461. This confirms that predicting the CBL of corroded WTSI columns in pre-engineered steel buildings with these input and output parameters is meaningful.

4 The Developed ANN Models

4.1 Background of ANN Algorithm

ANN model has been extensively employed to solve engineering problems (Nguyen et al., 2021a, b; Zorlu et al., 2008; Nguyen et al., 2021a, b, c; Patel & Mehta, 2018; Patil & Subbareddy, 2002). Fundamentally, ANN is one of the computing systems, which can constitute the human

Table 1 Statistical properties of the data sets

Properties	Unit	Min	Mean	Max	Standard deviation (SD)	Coefficient of variation (CV)
H	mm	2500.00	4957.90	9000.00	1755.92	0.35
$h_{c,\min}$	mm	200.00	284.09	460.00	46.87	0.16
$h_{c,\max}$	mm	240.00	365.91	500.00	56.66	0.15
$h_{b,\min}$	mm	220.00	314.35	490.00	47.81	0.15
$h_{b,\max}$	mm	270.00	411.37	560.00	58.52	0.14
b_f	mm	150.00	233.16	410.00	47.94	0.21
t_f	mm	10.00	30.63	50.00	12.11	0.40
t_w	mm	8.00	18.16	30.00	6.43	0.35
L_b	mm	10,000.00	19,124.35	30,000.00	5842.53	0.31
E	MPa	205.00	211.41	220.00	3.42	0.02
P_{cr}	kN	38.84	132,726.71	9751.03	18,741.81	1.92

brain. An ANN model is assembled based on neurons (i.e., connected units), which can receive and transfer signal to other neurons in the network. Neurons and their connections contain weights and biases that are used for adjusting the learning process. A typical ANN model includes three layers: (1) input layer, which contain input parameters; (2) hidden layer(s), and (3) output layer (i.e., predicted result). In this study, the back-propagation neural network and a Levenberg–Marquardt algorithm were employed to construct the predicted ANN model. The mathematical representation has been expressed by the following form.

$$\begin{aligned} &f : X \in R^D \rightarrow Y \in R^1 \\ &f(X) = f_0\left(b_2 + W_2\left(f_h\left(b_1 + W_1X\right)\right)\right) \end{aligned} \tag{9}$$

where b_1, W_1, and f_h are the bias, the weight, and the activation function of the hidden layer, respectively; b_2, W_2, and f_0 represent the bias, the weight, and the activation function of the output layer, respectively.

The used activation function in the hidden layer was a nonlinear function, namely *tansig* function, expressed by Eq. (10). And, a linear function, so-called *purelin* function, was employed for the output layer (Nikbin et al., 2017), as shown in Eq. (11), and shown in Fig. 5.

$$\mathrm{tansig}(x) = \frac{2}{(1 + \mathrm{epx}(-2x))} - 1 \tag{10}$$

$$\mathrm{purelin}(x) = x \tag{11}$$

Moreover, for getting a good convergence and setting the inputs in a comparable range, the input and output parameters should be normalized in the [− 1, 1] range (Golafshani & Ashour, 2016). This procedure can be implemented by Eq. (12).

$$X_n = 2 \times \frac{\left(X - X_{\min}\right)}{\left(X_{\max} - X_{\min}\right)} - 1 \tag{12}$$

where X_n is the normalized sample; $X_{\max}$, $X_{\min}$, and X are the maximum, minimum and value of the dataset under consideration, respectively.

The training process of the network was performed continuously until a convergence was achieved. For that, the mean square error (MSE) was utilized to quantify the convergence. The MSE can be calculated by Eq. (13).

$$\mathrm{MSE} = \min_{b_1,b_2,W_1,W_2} \frac{1}{N} \sum_{i=1}^{N} e_i^2 \tag{13}$$

where e_i is the difference between the predicted output and the experiment values; N is number of data sets.

4.2 Indicators for Performance Evaluation of ANN Model

To quantify the performance of the ANN model three statistical indicators, which are R^2, $RMSE$, and $a20-$ index, were employed (Zorlu et al., 2008). The definitions of these parameters are as follows.

$$R^2 = 1 - \left(\frac{\sum_{i=1}^{N} \left(t_i - o_i\right)^2}{\sum_{i=1}^{N} \left(t_i - \overline{o}\right)^2} \right) \tag{14}$$

$$\mathrm{RMSE} = \sqrt{\left(\frac{1}{n}\right) \sum_{i=1}^{N} \left(t_i - o_i\right)^2} \tag{15}$$

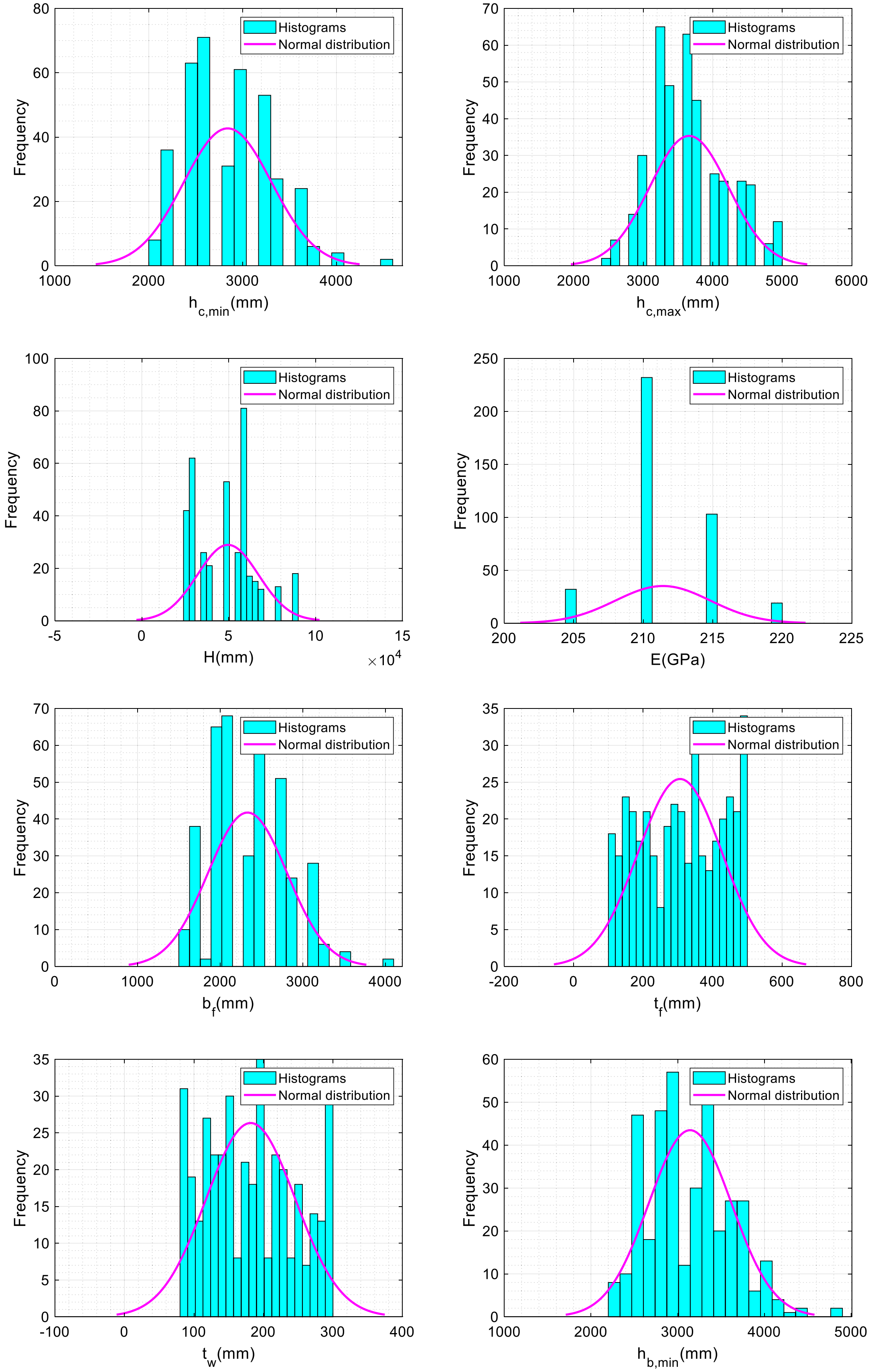

Fig. 3 Histograms of input and output parameters

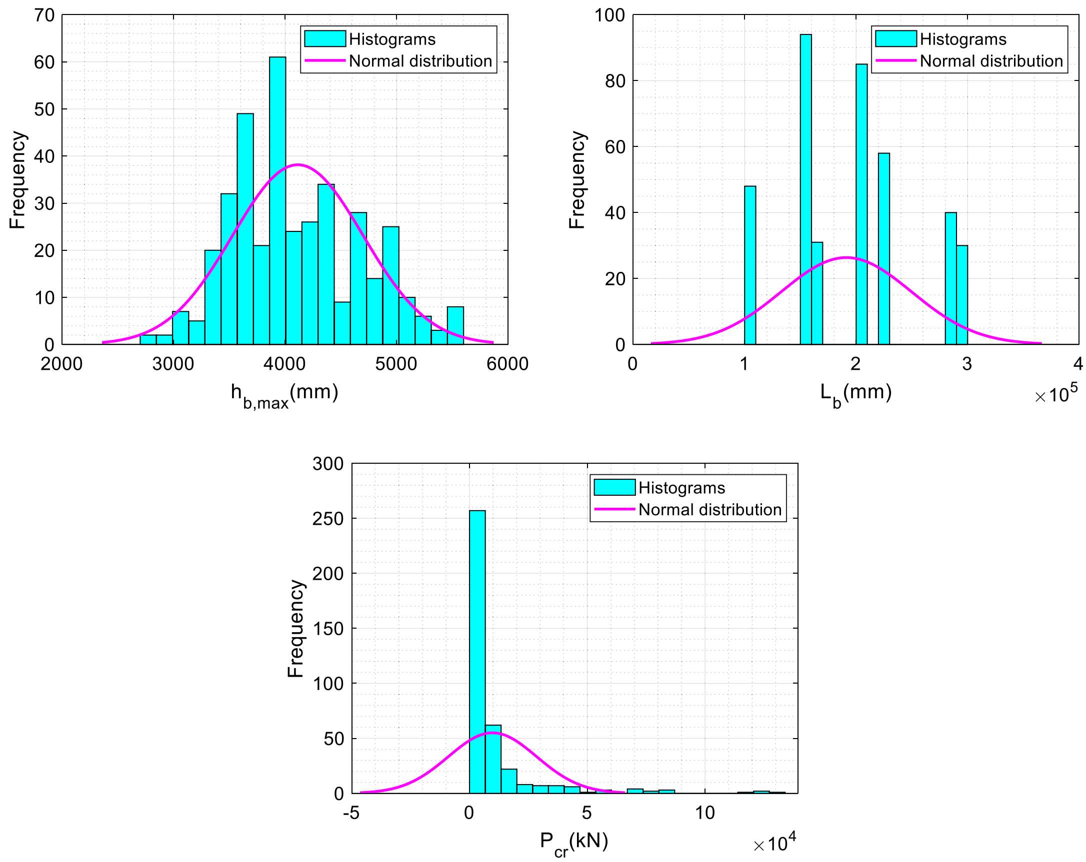

Fig. 3 (continued)

$$a20 - \text{index} = \frac{n20}{N} \tag{16}$$

where t_i and o_i represent the target and output of i^{th} data point, respectively; $\overline{o}$ is the mean of output data samples; N is the number of samples; $n20$ is the number of samples with the ratio of the experimental value to the predicted value between the range [0.8–1.2].

4.3 Performance of ANN Models with the Dataset

In this study, the input variables are divided into three sets: 70% training, 15% validation, and 15% testing. The number of neurons in the hidden layers are tested from 5 to 10. As a result, the optimal model is obtained based on the three indicators (i.e., R^2, RMSE, and $a20$-index) with 8 neurons in the hidden layer. The proposed ANN model is shown in Fig. 6.

Figure 7 and Table 2 show the training results of the ANN model. It can be observed that the training process stopped at the 34th epoch with the MSE value of 0.00014. This implies that the developed ANN model has a good performance with respect to the input data sets.

Figure 8 provides the regression results of the training, testing, validation, and all data of the ANN model. The R^2 values of the training, testing, and validation data were 0.99975, 0.99916, and 0.99951, respectively. It is shown to be very close to unity. This highlighted that the ANN model was capable of predicting CBL of the WTSI columns in pre-engineered steel buildings.

Table 2 summarizes the calculated values of R^2, RMSE, and *a*20-*index*. The statistical indicators including minimum, maximum, mean, standard deviation (SD), and coefficient of variation (CV) of the ratio predicted/dataset were also obtained in the table. It can be found that the mean value was very close to 1.0. The results confirmed that the proposed ANN model structure can estimate the critical buckling load of the WTSI columns accurately.

	hc,min	*hc,max*	*H*	*a*	*E*	*bf*	*tf*	*t-w*	*hb,min*	*hb,max*	*L*	*P*
hc,min	1.000	0.442	-0.002	0.415	-0.023	-0.082	-0.086	-0.023	0.978	0.423	-0.099	-0.260
hc,max	0.442	1.000	-0.060	-0.314	0.032	-0.001	-0.049	0.077	0.427	0.974	-0.052	0.461
H	-0.002	-0.060	1.000	0.394	0.006	-0.055	0.062	-0.044	-0.006	-0.048	-0.009	-0.384
a	0.415	-0.314	0.394	1.000	-0.090	-0.127	-0.070	-0.013	0.396	-0.318	-0.052	-0.407
E	-0.023	0.032	0.006	-0.090	1.000	-0.012	0.042	-0.027	-0.028	0.030	0.037	0.018
bf	-0.082	-0.001	-0.055	-0.127	-0.012	1.000	-0.093	-0.093	-0.068	0.003	0.081	0.120
tf	-0.086	-0.049	0.062	-0.070	0.042	-0.093	1.000	-0.044	-0.065	-0.054	-0.030	0.097
t-w	-0.023	0.077	-0.044	-0.013	-0.027	-0.093	-0.044	1.000	-0.027	0.078	-0.067	0.066
hb,min	0.978	0.427	-0.006	0.396	-0.028	-0.068	-0.065	-0.027	1.000	0.420	-0.095	-0.254
hb,max	0.423	0.974	-0.048	-0.318	0.030	0.003	-0.054	0.078	0.420	1.000	-0.051	0.443
L	-0.099	-0.052	-0.009	-0.052	0.037	0.081	-0.030	-0.067	-0.095	-0.051	1.000	0.010
P	-0.260	0.461	-0.384	-0.407	0.018	0.120	0.097	0.066	-0.254	0.443	0.010	1.000

Fig. 4 Correlation between input and output parameters

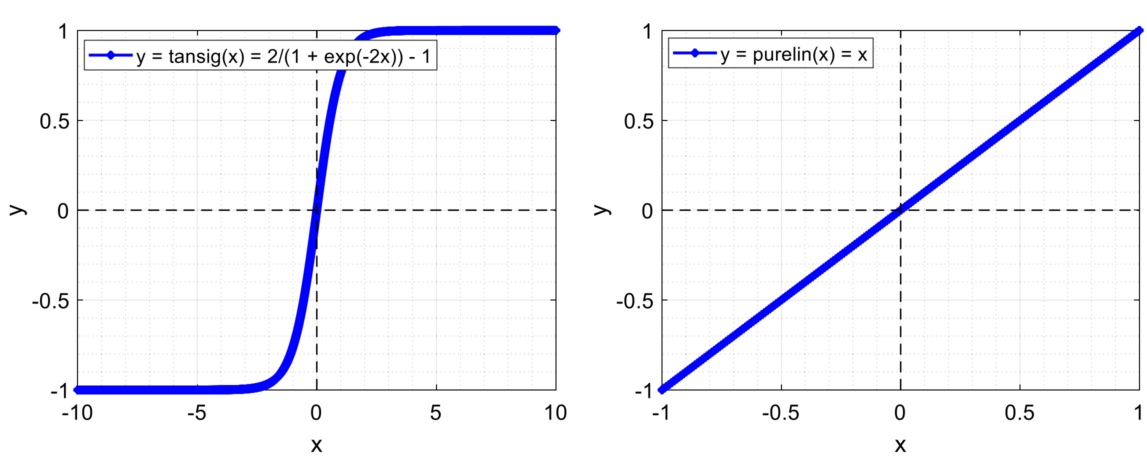

Fig. 5 Activation functions for ANN model: tansig(x) and purelin(x)

Fig. 6 The proposed ANN model structure

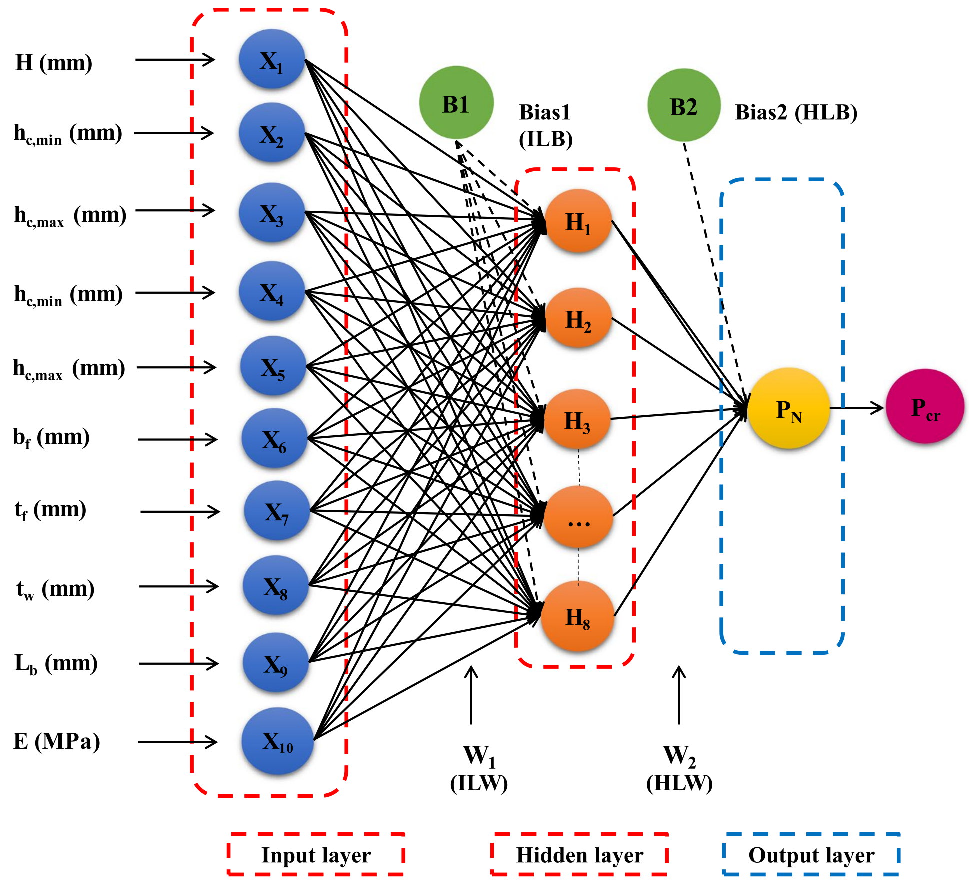

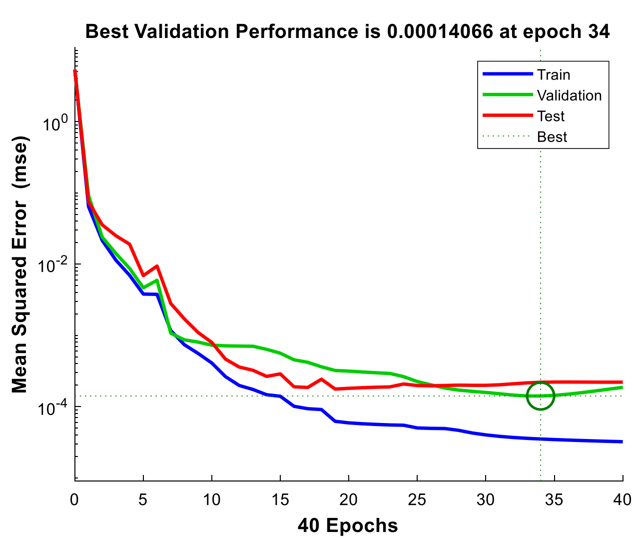

Fig. 7 Performance of ANN model

5 Prediction of the CBL of Corroded WTSI Columns

5.1 Corrosion Model

There are several typical corrosion models used in civil engineering to assess and predict the corrosion of structures. Here are a few common models:

(1) Uniform corrosion model: This model assumes that corrosion occurs uniformly across the entire surface of the steel structure. It is often used for initial estimates and simple structures where environmental conditions are consistent and there are no significant variations in exposure conditions.

(2) Localized corrosion model: This model considers the occurrence of corrosion in specific areas or localized regions of the structure. Examples include pitting corrosion, crevice corrosion, and galvanic corrosion.

Table 2 Performance of ANN model

	R^2	*RMSE (kN)*	*a20-index*	$P_{cr}/P_{cr}^{predict}$				
				Min	Mean	Max	SD	CV
All data	0.9995	98.738	0.9018	0.1410	0.9715	1.5509	0.1725	0.1775
Training	0.9997	96.705	0.9111	0.4310	1.0031	1.5509	0.1223	0.1219
Validation	0.9993	103.200	0.9138	0.4981	0.9783	1.4059	0.1309	0.1338
Testing	0.9991	103.402	0.8448	0.1410	0.9530	1.3620	0.2061	0.2162

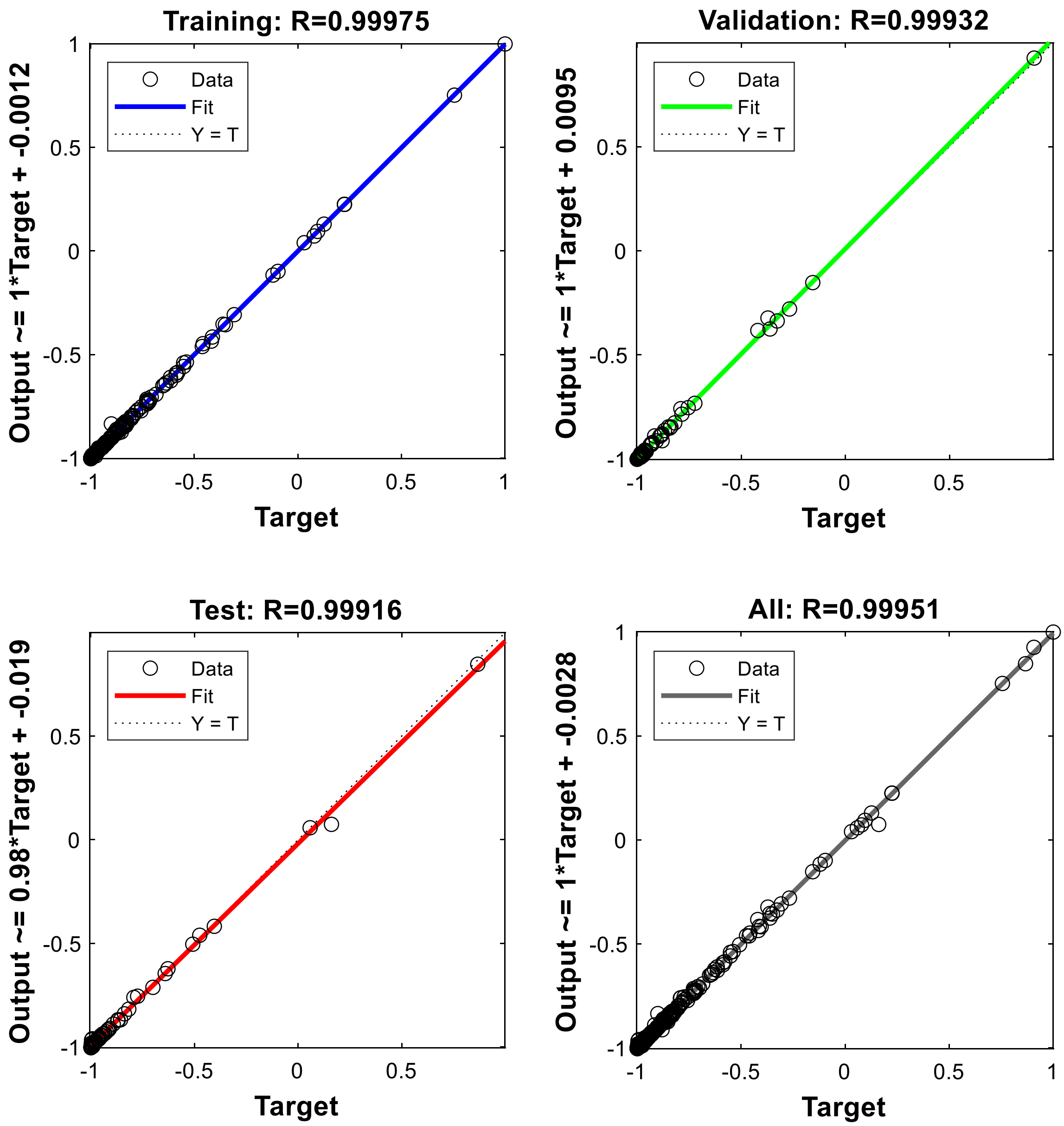

Fig. 8 Regression results of the training, testing, validation, and all data

Localized corrosion models are useful for assessing the vulnerability of specific areas to corrosion and identifying potential failure points.

(3) Atmospheric corrosion model: This model focuses on the corrosion of structures exposed to the atmosphere. It considers environmental factors such as humidity, temperature, rainfall, and air pollutants. Atmospheric

Table 3 Average values of corrosion parameters A and B for carbon steel and weathering steel

Environment	Carbon steel		Weathering steel	
	A	*B*	*A*	*B*
Rural	34.0	0.65	33.3	0.50
Urban	80.2	0.59	50.7	0.57
Marine	70.6	0.79	40.2	0.56

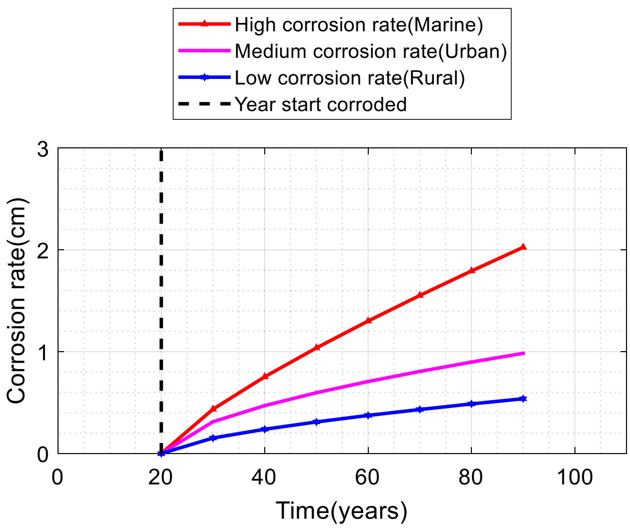

Fig. 9 The used corrosion rate model

corrosion models are commonly used for outdoor structures such as bridges, towers, and pipelines.

(4) Reinforcement corrosion model: This model specifically addresses the corrosion of reinforcement bars in reinforced concrete structures. It considers factors such as concrete cover thickness, chloride ingress, and moisture content to predict the initiation and propagation of corrosion in the reinforcement.

It is important to note that these models are simplified representations of the complex corrosion processes that occur in civil engineering structures. For this study, the corrosion model proposed by Komp (1987) is adopted due to its simplicity (Morcillo et al., 2013). Additionally, it is very popular to employ a power function to estimate the long-term atmospheric corrosion of steel (Knotkova et al., 2010). The Komp model (1987) is expressed by

$$D(t) = A.t^{B} \tag{17}$$

where $D(t)$ is the corrosion depth; t is the exposing time (year); A is the corrosion rate in the first year of exposure, B is the corrosion rate long-term decrease. A and B are constants, which depend on the environmental conditions, as provided in Table 3.

For predicting the CBL of corroded WTSI columns, the proposed ANN model was combined with the corrosion model developed by Komp (1987), in which the assumption of uniform corrosion started from the 20th year (Tran et al., 2022), as shown in Fig. 9.

5.2 Prediction of the CBL of Corroded WTSI Columns

The procedure for predicting CBL of corroded WTSI columns is conducted by the following steps (Fig. 10).

- Step 1. Determine the input parameters of WTSI columns and set the corroded time.
- Step 2. Calculate the damaged stiffness and cross-section loss accounting for corrosion.
- Step 3. Normalize datasets after considering steel corrosion.
- Step 4. Determine the CBL of the corroded WTSI columns in pre-engineered steel buildings by the developed ANN model and the data considered corrosion.

5.3 The Prediction Formula for CBL of WTSI Columns

In the practical design, a simplified tool should be used. A formula to calculate the CBL of corroded WTSI columns was built based on the performance of the ANN model. For that, the study used activation function, weight, biases vector, and normalized Eq. (12), to propose a formula, as follows.

$$P_{\mathrm{cr}}^{\mathrm{Pre}} = 66382.80 \times \left(P_{cr}^{N} + 1\right) + 38.83\,(kN) \tag{18}$$

where the coefficients 66,382.80 and 38.83 are half the values of the maximum and minimum CBL of corroded WTSI columns in the input datasets, respectively. P_{cr}^{N} is the normalized CBL of WTSI columns, determined by the following equation.

$$\begin{aligned} P_{cr}^{N} &= h_0 + \sum_{i=1}^{8} h_i H_i \; H_i \\ &= \tanh\left(c_{i0} + c_{i1}X_1 + c_{i2}X_2 + \ldots + c_{i10}X_{10}\right) \end{aligned} \tag{19}$$

where the h_0, h_i and $c_{i0}, \ldots, c_{i10}$ are coefficients shown in Table 4. Those coefficients are obtained from the ANN model.

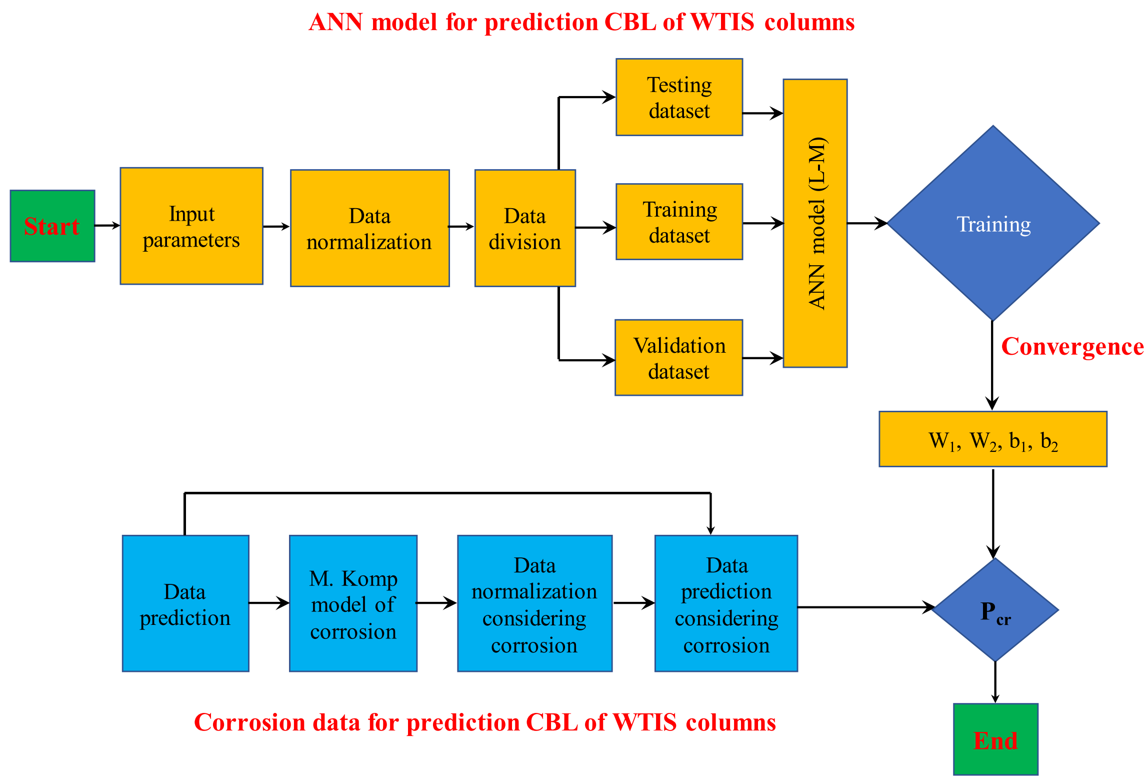

Fig. 10 Flowchart of prediction of the CBL of corroded WTSI columns

Table 4 Coefficients for Eq. (19)

i	h_i	c_{io}	c_{i1}	c_{i2}	c_{i3}	c_{i4}	c_{i5}	c_{i6}	c_{i7}	c_{i8}	c_{i9}	c_{i10}
0	0.9095											
1	0.3272	0.0096	−1.1715	0.9283	−0.8594	0.1019	−0.5656	−0.3871	−0.2138	−1.2736	0.3592	0.0188
2	−0.5136	0.0087	−0.5403	1.1153	1.3927	0.2059	1.1006	1.1766	0.5732	0.3596	0.9640	0.1321
3	−0.6649	0.0002	1.1956	−1.9446	1.8708	−1.0667	−1.6123	−1.7571	0.9151	2.2097	−1.2565	−0.4543
4	1.4698	−0.2580	1.3392	−1.4046	0.8047	−0.0441	−0.3844	−0.1987	0.0101	−0.0335	−0.0040	0.0018
5	3.6635	−2.3689	1.3069	−0.8489	1.9776	−0.0146	−0.4644	−0.2119	−0.0375	−0.3775	−0.3483	−0.0326
6	−0.6416	0.0026	−1.1118	0.9534	−0.2025	−2.0412	0.2942	−0.3119	1.4336	−0.4933	1.5271	−0.5141
7	3.5850	0.1875	1.6922	−0.4226	0.9268	0.1227	−0.5108	1.3083	0.0446	0.0023	−1.8007	0.1379
8	2.2530	0.5314	0.3499	0.4146	1.4818	−0.0972	−0.5714	−0.2195	−0.0302	−0.4712	−0.4846	−0.0442

5.4 Graphical User Interface

A graphical user interface (GUI) program was developed using MATLAB (Mathworks 2018), as shown in Fig. 11. This tool provides a convenient platform to calculate the CBL of the corroded WTSI columns for design practices. Eleven input parameters, which are the column height (H), the maximum cross-section height of column ($h_{c,\max}$), the minimum cross-section height of column ($h_{c,\min}$), the flange width (b_f), the maximum cross-section height of beam ($h_{b,\max}$), the minimum cross-section height of beam ($h_{b,\min}$), the flange thickness (t_f), the web thickness (t_w), the bay width of frame (L_b), elastic modulus of material (E), and corrosion time, are required. The developed GUI is freely accessible and easy to use. This GUI tool was created using the ANN model, thus the predictive accuracy was verified and presented in the previous section.

6 Numerical Investigation

Considering a two-dimensional frame of the pre-engineered steel building, which contains input parameters in Table 5. Figures 12 and 13 show the plan and elevation as

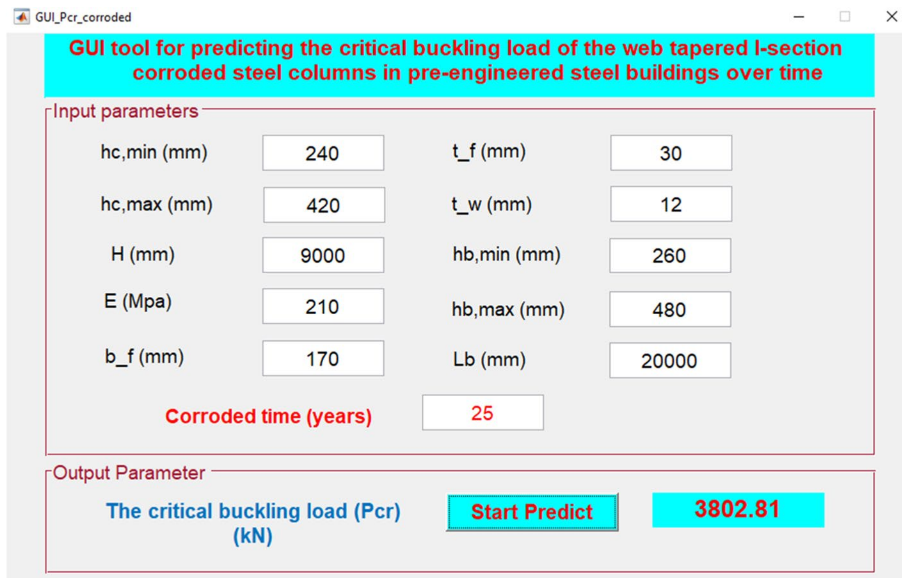

Fig. 11 GUI for calculating CBL of corroded WTSI columns

Table 5 Input variables for the numerical investigation

H (mm)	$h_{c,\min}$ (mm)	$h_{c,\max}$ (mm)	$h_{b,\min}$ (mm)	$h_{b,\max}$ (mm)	b_f (mm)	t_f (mm)	t_w (mm)	L_b (mm)	E MPa
4957.90	284.09	365.91	314.35	411.37	233.16	30.63	18.16	19,124.35	211.41

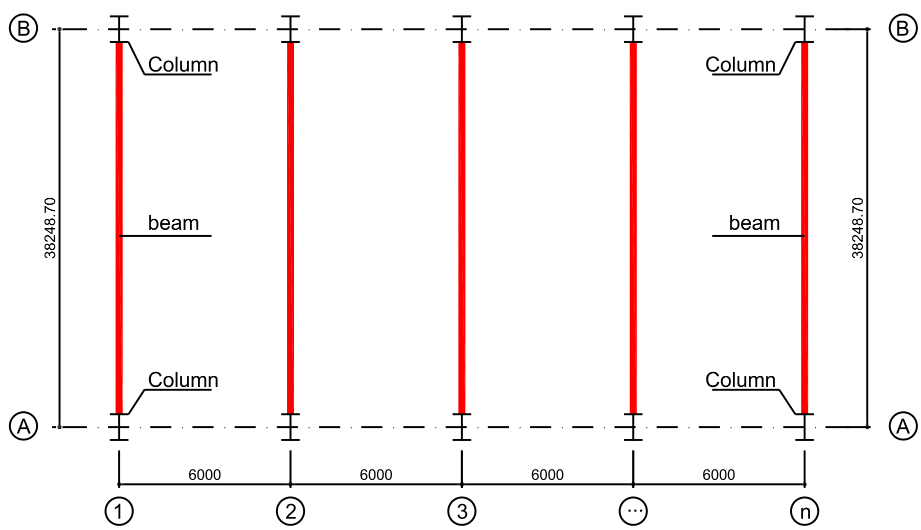

Fig. 12 Plan of the investigated pre-engineering steel building

well as cross-sectional dimensions of the pre-engineering steel frame with WTSI columns. The service life of the CBL of corroded WTSI columns is considered until the 100th year. Meanwhile metal corrosion of WTSI columns started from the 20th year. The CBL of WTSI columns decreases with time, as shown in Fig. 14. Based on this figure, the CBL of corroded WTSI columns is reduced approximately 26.66% after 100 years. It proves that the study of CBL of corroded WTSI columns has scientific and practical significance. This finding can be suggested to the existing design codes.

7 Effect of Input Variables on the CBL of WTSI Columns

The effect of input variable on the CBL of WTSI columns is helpful for managers and designers in determining the maintenance or demolition of structures. The input parameters were changed from minimum (L) to maximum (H) limits. At the time to assess the Parameter X_i, other parameters were remaining at the medium value. All databases are shown in Table 6.

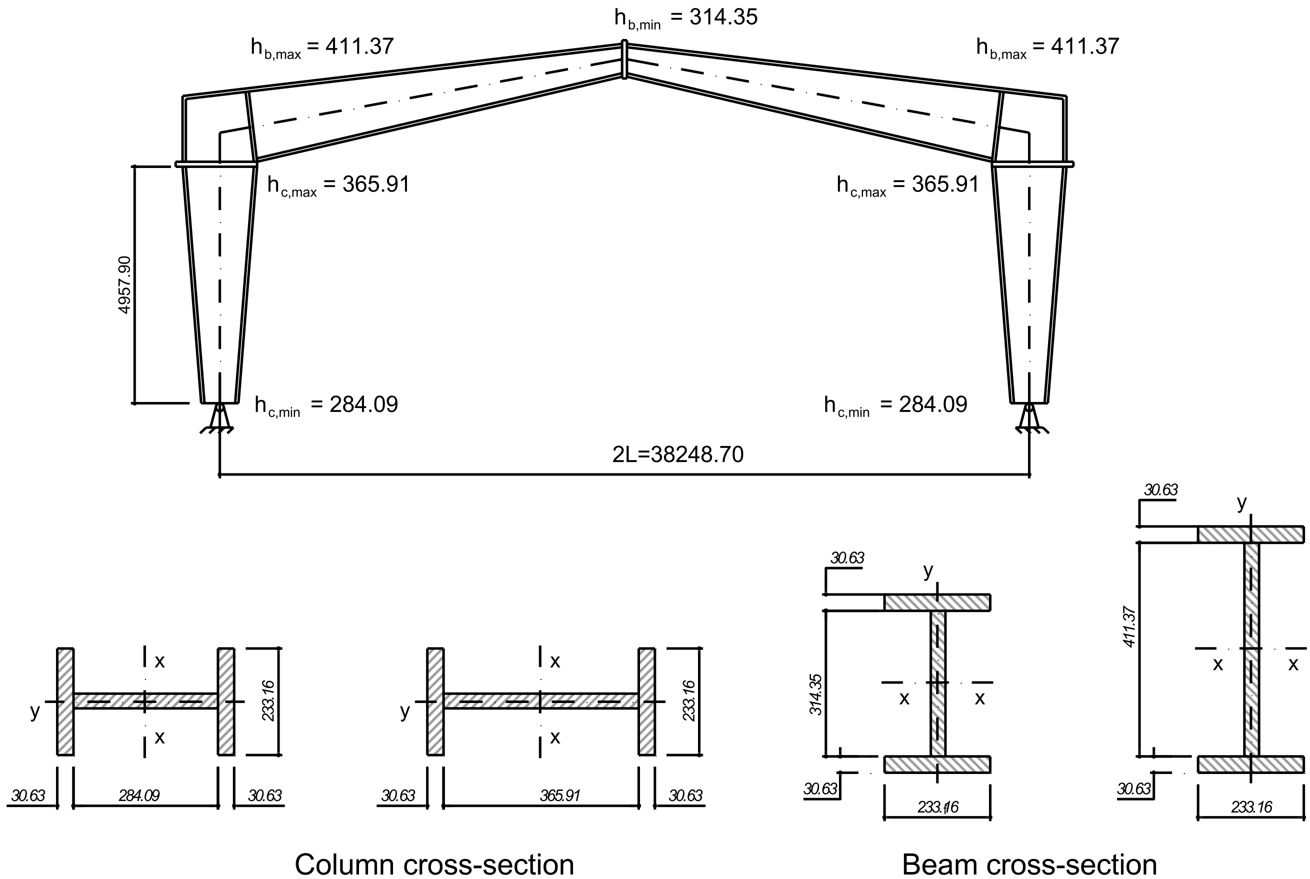

Fig. 13 Dimensions of the pre-engineering steel frame with WTSI columns

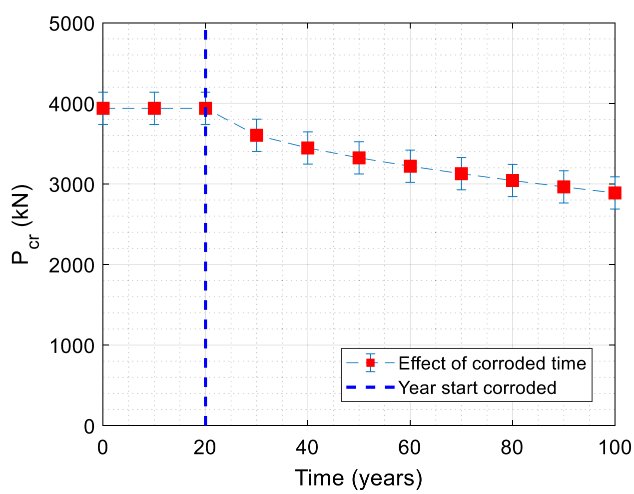

Fig. 14 The CBL of WTSI columns decreases with time

Table 6 The range of input parameters

Input variables	L	LM	M	MH	H
H	2500.00	3728.95	4957.90	6978.95	9000.00
$h_{c,\min}$	200.00	242.05	284.09	372.05	460.00
$h_{c,\max}$	240.00	302.96	365.91	432.96	500.00
$h_{b,\min}$	220.00	267.18	314.35	402.18	490.00
$h_{b,\max}$	270.00	340.69	411.37	485.69	560.00
b_f	150.00	191.58	233.16	321.58	410.00
t_f	10.00	20.32	30.63	40.32	50.00
t_w	8.00	13.08	18.16	24.08	30.00
L_b	10,000.00	14,562.18	19,124.35	24,562.18	30,000.00
E	205.00	208.21	211.41	215.71	220.00

H: High; MH: Middle high; M: Medium; LM: Middle low; L: Low)

Figure 15 presents the effects of input parameters on the CBL of corroded WTSI columns. It can be observed that the CBL tended to increase with the increment of b_f, t_f, t_w, and $h_{c,\max}$. Meanwhile the CBL was reduced with the increment of $h_{b,\max}$, $h_{b,\min}$, H, and $h_{c,\min}$. Moreover, the CBL of corroded WTSI columns kept constant with the increment of L_b and E.

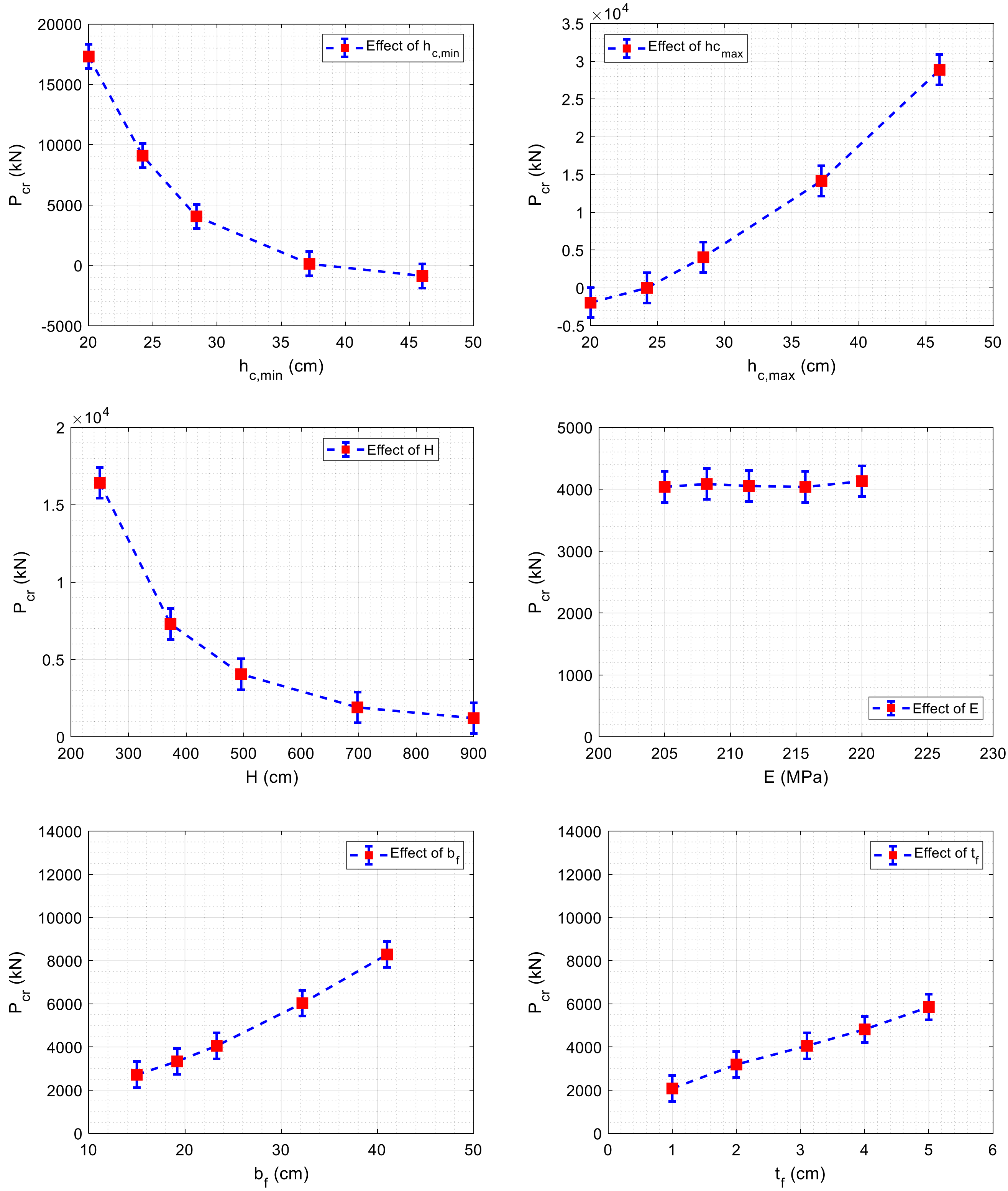

Fig. 15 Effects of input variables on the CBL of WTSI columns

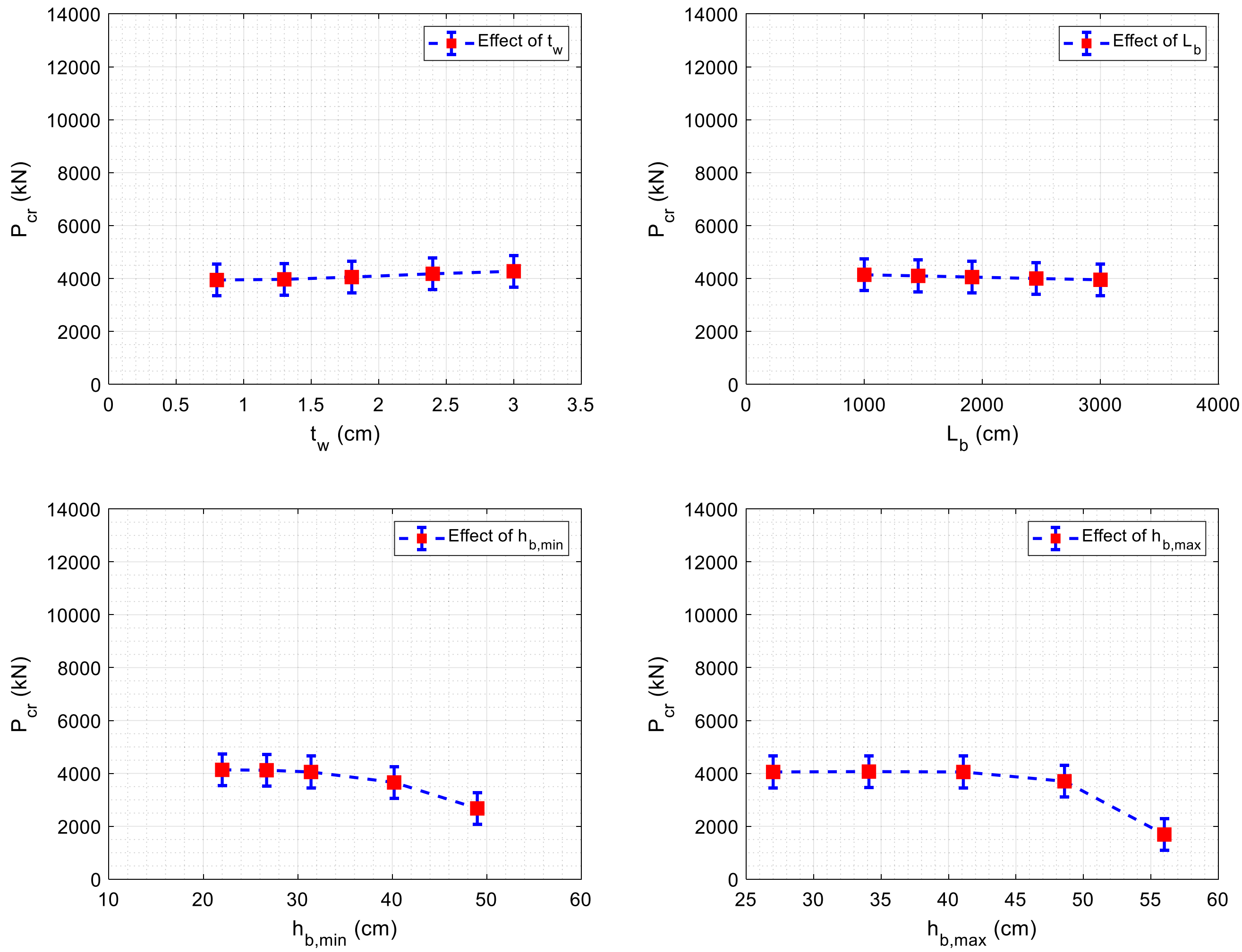

Fig. 15 (continued)

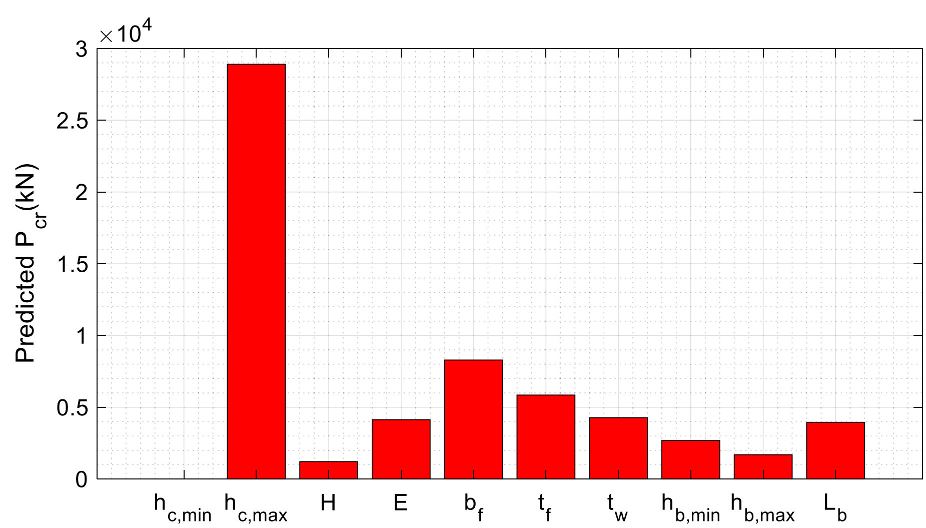

Fig. 16 The sensitivity of input variables on the CBL of WTSI columns

8 Sensitivity Analysis

Figure 16 shows the sensitivity of input parameters on the CBL of corroded WTSI columns. Noting that P_{cr} obtained in the figure is the maximum value corresponding to each input parameter. The maximum cross-section height of column ($h_{c,\max}$) has the highest influence on the CBL, followed by flange width, (b_f) and the flange thickness (t_f). Meanwhile, the column height (H) has a negative effect on the CBL of the columns.

9 Conclusions

This study developed an artificial neural network (ANN) to estimate the critical buckling load (CBL) of corroded web tapered I-section steel (WTSI) columns. A total of 387 data sets were analytically generated to construct the ANN model. A predictive process for calculating CLB of the corroded WTSI columns was proposed using the ANN model and previous corrosion model. The following conclusions are obtained.

- A procedure for predicting CBL of corroded WTSI columns is proposed based on the ANN model and Newton–Raphson method, in which the datasets are created using the analytical approach.
- The developed ANN model predicts CBL of the corroded WTSI columns accurately with R^2 values of the training, testing, and validation data are 0.99975, 0.99916, and 0.99951, respectively, and the *a20*-index is very close to 1.0.
- A practical formula for calculating the CBL of corroded WTSI columns in pre-engineered steel buildings is proposed.
- A graphical user interface tool is developed to facilitate the CBL calculation of the corroded WTSI columns in pre-engineered steel buildings.
- The effects of input variables on the CBL of corroded WTSI columns in pre-engineered steel buildings are evaluated. The maximum cross-section height of column ($h_{c,\max}$) is the most influential variable. Whereas the column height (H) has a negative influence on the calculated CBL.

Declarations

Conflicts of interest The authors declare that they have no conflicts of interest.

References

Andalib, Z., Caputo, P., Dorafshan, S., Maguire, M., & Collins, W. Investigation into the behavior of an open web steel joist bridge. In *Proceedings of the 2018 International Bridge Conference, National Harbor, MD, USA, 2018a*

Andalib, Z., Kafi, M. A., Kheyroddin, A., & Bazzaz, M. (2014). Experimental investigation of the ductility and performance of steel rings constructed from plates. *Journal of Constructional Steel Research, 103*, 77–88.

Andalib, Z., Kafi, M. A., Kheyroddin, A., Bazzaz, M., & Momenzadeh, S. (2018b). Numerical evaluation of ductility and energy absorption of steel rings constructed from plates. *Engineering Structures, 169*, 94–106.

Bazzaz, M., Andalib, Z., Kafi, M. A., & Kheyroddin, A. (2015a). Evaluating the performance of OBS-CO in steel frames under monotonic load. *Journal of Earthquakes and Structures, 8*(3), 697–710.

Bazzaz, M., Andalib, Z., Kheyroddin, A., & Kafi, M. A. (2015b). Numerical comparison of the seismic performance of steel rings in off-centre bracing system and diagonal bracing system. *Journal of Steel and Composite Structures, 19*(4), 917–937.

Bazzaz, M., Kafi, M. A., Kheyroddin, A., Andalib, Z., & Esmaeili, H. (2014). Evaluating the seismic performance of off-centre bracing system with circular element in optimum place. *International Journal of Steel Structures, 14*(2), 293–304.

Bazzaz, M., Kheyroddin, A., Kafi, M. A., & Andalib, Z. (2012). Evaluation of the seismic performance of off-centre bracing system with ductile element in steel frames. *Steel & Composite Structures, 12*(5), 445–464.

CEN, E. (2005). *1-1-Eurocode 3: Design of steel structures-Part 1–1: General rules and rules for buildings*. European Committee for Standardization.

Chico, B., De la Fuente, D., Díaz, I., Simancas, J., & Morcillo, M. (2017). Annual atmospheric corrosion of carbon steel worldwide. An integration of ISOCORRAG. *ICP/UNECE and MICAT databases. Materials, 10*(6), 601.

Eurocode, E. (1996). 3: Design of steel structures–Part 1.4: General rules–Supplementary rules for stainless steels. European Committee for Standardization. ENV 1993–1–4, CEN, Brussels.

Flah, M., Nunez, I., Ben Chaabene, W., & Nehdi, M. L. (2021). Machine learning algorithms in civil structural health monitoring: A systematic review. *Archives of Computational Methods in Engineering, 28*, 2621–2643.

Gardner, L., & Nethercot, D. A. (2005). *Designers' Guide to EN 1993–1–1 Eurocode 3: Design of Steel Structures: General Rules and Rules for Buildings*: Thomas Telford Publishing.

Golafshani, E. M., & Ashour, A. (2016). A feasibility study of BBP for predicting shear capacity of FRP reinforced concrete beams without stirrups. *Advances in Engineering Software, 97*, 29–39.

Ha, N. T. (2019). Reliability assessment of frame steel considering semi-rigid connections. *Journal of Materials and Engineering Structures, 6*(1), 119–126.

Ilter, E., Celik, O. C., & Unlu, A. (2020). Multi-criteria performance evaluation of a glass panel system using full-scale experimental data. *Architectural Science Review, 63*(6), 507–525.

Knotkova, D., Boschek, P., & Kreislova, K. (1995). Results of ISO CORRAG program: processing of one-year data in respect to corrosivity classification. In *Atmospheric Corrosion*: ASTM International.

Knotkova, D., Kucera, V., Dean, S. W., & Boschek, P. (2002). Classification of the corrosivity of the atmosphere—standardized classification system and approach for adjustment. In *Outdoor atmospheric corrosion*: ASTM International.

Knotkova, D., Dean, S. W., & Kreislova, K. (2010). *ISOCORRAG, International Atmospheric Exposure Program: Summary of*

Results: Developed by ISO/TC 156/WG 4, Atmospheric Corrosion Testing and Classification of Corrosivity of Atmosphere: ASTM International.

Komp, M. (1987). Atmospheric corrosion ratings of weethering steels-calculation and significance. *Materials Performance, 26*(7), 42–44.

Kucera, V., Tidblad, J., Kreislova, K., Knotkova, D., Faller, M., Reiss, D., et al. (2007). UN/ECE ICP materials dose-response functions for the multi-pollutant situation. In *Acid Rain-Deposition to Recovery* (pp. 249–258): Springer.

Landolfo, R., Cascini, L., & Portioli, F. (2010). Modeling of metal structure corrosion damage: A state of the art report. *Sustainability, 2*(7), 2163–2175.

Li, X.-X. Design of tapered beam-columns. In *Proceedings of the 2008 Annual Stability Conference, Tennessee, USA., 2008*

Marques, L., Da Silva, L. S., & Rebelo, C. (2014a). Rayleigh Ritz procedure for the determination of the critical load of tapered columns. *Steel and Composite Structures, 16*(1), 45–58.

Marques, L., da Silva, L. S., Rebelo, C., & Santiago, A. (2014b). Extension of EC3-1-1 interaction formulae for the stability verification of tapered beam-columns. *Journal of Constructional Steel Research, 100*, 122–135.

Marques, L., Taras, A., da Silva, L. S., Greiner, R., & Rebelo, C. (2012). Development of a consistent buckling design procedure for tapered columns. *Journal of Constructional Steel Research, 72*, 61–74.

Mathworks, I. (2018). MATLAB and statistics toolbox release 2018b. *Natick (Massachusetts, United States)*.

Mikhailov, A., Tidblad, J., & Kucera, V. (2004). The classification system of ISO 9223 standard and the dose–response functions assessing the corrosivity of outdoor atmospheres. *Protection of Metals, 40*(6), 541–550.

Morcillo, M. (1995). *Atmospheric corrosion in Ibero-America: the MICAT project*. In Atmospheric corrosion: ASTM International.

Morcillo, M., Chico, B., Díaz, I., Cano, H., & De la Fuente, D. (2013). Atmospheric corrosion data of weathering steels. *A Review. Corrosion Science, 77*, 6–24.

Naser, M. (2023). Machine learning for all! Benchmarking automated, explainable, and coding-free platforms on civil and environmental engineering problems. *Journal of Infrastructure Intelligence and Resilience, 2*(1), 100028.

Ngoc-Long, T., & Ha, T. (2020). The effect of metal corrosion on the structural reliability of the Pre-Engineered steel frame. *Journal of Materials and Engineering Structures, 7*(2), 155–165.

Nguyen, D.-D., Tran, V.-L., Ha, D.-H., Nguyen, V.-Q., & Lee, T.-H. (2021). A machine learning-based formulation for predicting shear capacity of squat flanged RC walls. *In Structures*. https://doi.org/10.1016/j.istruc.2020.12.054

Nguyen, Q.-V. (2007). *Buckling of web-tapered I-section columns in steel frames*. Construction Publishing House.

Nguyen, T.-H., Tran, N.-L., & Nguyen, D.-D. (2021). Prediction of axial compression capacity of cold-formed steel oval hollow section columns using ANN and ANFIS models. *International Journal of Steel Structures*. https://doi.org/10.1007/s13296-021-00557-z

Nguyen, T.-H., Tran, N.-L., & Nguyen, D.-D. (2021). Prediction of critical buckling load of web tapered i-section steel columns using artificial neural networks. *International Journal of Steel Structures, 24*, 1–23.

Nikbin, I. M., Rahimi, S., & Allahyari, H. (2017). A new empirical formula for prediction of fracture energy of concrete based on the artificial neural network. *Engineering Fracture Mechanics, 186*, 466–482. https://doi.org/10.1016/j.engfracmech.2017.11.010

Panchenko, Y. M., & Marshakov, A. I. (2017). Prediction of first-year corrosion losses of carbon steel and zinc in continental regions. *Materials, 10*(4), 422.

Patel, V. M., & Mehta, H. B. (2018). Thermal performance prediction models for a pulsating heat pipe using Artificial Neural Network (ANN) and Regression/Correlation Analysis (RCA). *Sādhanā, 43*(11), 1–16. https://doi.org/10.1007/s12046-018-0954-3

Patil, S. B., & Subbareddy, N. (2002). Neural network based system for script identification in Indian documents. *Sādhanā, 27*(1), 83–97. https://doi.org/10.1007/BF02703314

Reich, Y. (1997). Machine learning techniques for civil engineering problems. *Computer-Aided Civil and Infrastructure Engineering, 12*(4), 295–310.

Roberge, P., Klassen, R., & Haberecht, P. (2002). Atmospheric corrosivity modeling—A review. *Materials & Design, 23*(3), 321–330.

Secer, M., & Uzun, E. T. (2017). Corrosion damage analysis of steel frames considering lateral torsional buckling. *Procedia Engineering, 171*, 1234–1241.

Simões da Silva, L., Simões, R., & Gervásio, H. (2010). *Design of Steel structures*. ECCS Press and Ernst & Sohn.

Standard, B. (2002). Eurocode—Basis of structural design. EN 1990.

Thai, H.-T. Machine learning for structural engineering: A state-of-the-art review. In *Structures, 2022* (Vol. 38, pp. 448–491): Elsevier

Tidblad, J., Kucera, V., Mikhailov, A. A., Henriksen, J., Kreislova, K., Yates, T., et al. (2001). UN ECE ICP materials: Dose-response functions on dry and wet acid deposition effects after 8 years of exposure. In *Acid rain 2000* (pp. 1457–1462): Springer.

Tidblad, J. (2012). Atmospheric corrosion of metals in 2010–2039 and 2070–2099. *Atmospheric Environment, 55*, 1–6.

Tran, N.-L., & Nguyen, T.-H. Effect of Metal Corrosion on the Structural Reliability of the 3D Steel Frames. In *Proceedings of the 3rd International Conference on Sustainability in Civil Engineering, 2021* (pp. 39–44): Springer doi:https://doi.org/10.1007/978-981-16-0053-1_5.

Tran, N.-L., Nguyen, D.-D., & Nguyen, T.-H. (2022). Prediction of speed limit of cars moving on corroded steel girder bridges using artificial neural networks. *Sādhanā, 47*(3), 1–14.

Tran, V.-L., & Kim, S.-E. (2020). Efficiency of three advanced data-driven models for predicting axial compression capacity of CFDST columns. *Thin-Walled Structures, 152*, 106744. https://doi.org/10.1016/j.tws.2020.106744

Tran, V.-L., Thai, D.-K., & Kim, S.-E. (2019). Application of ANN in predicting ACC of SCFST column. *Composite Structures, 228*, 111332. https://doi.org/10.1016/j.compstruct.2019.111332

Vadyala, S. R., Betgeri, S. N., Matthews, J. C., & Matthews, E. (2022). A review of physics-based machine learning in civil engineering. *Results in Engineering, 13*, 100316.

Vakhshouri, B., & Nejadi, S. (2018). Prediction of compressive strength of self-compacting concrete by ANFIS models. *Neurocomputing, 280*, 13–22. https://doi.org/10.1016/j.neucom.2017.09.099

Zorlu, K., Gokceoglu, C., Ocakoglu, F., Nefeslioglu, H., & Acikalin, S. (2008). Prediction of uniaxial compressive strength of sandstones using petrography-based models. *Engineering Geology, 96*(3–4), 141–158. https://doi.org/10.1016/j.enggeo.2007.10.009